CHAPTER IV
RESULTS AND DISCUSSION

This chapter presents the results from two distinct samples: BFO on NSTO and a Gold Nanohole Array (AuNHA). The characteristics and properties of these materials were investigated using various techniques to examine the impact of nano-patterning. Additionally, the effect of UV irradiation on ferroelectricity is discussed.

4.1 Basic characterization

4.1.1 X-ray diffraction (XRD)

XRD was used to analyze the crystal structure of 7 different samples, including NSTO, FTO, BFO/NSTO, BFO/FTO both before and after annealing, and AuNHA sample. The main peaks of NSTO and FTO were visible in all samples. The unannealed BFO samples showed an amorphous phase with peaks at 2θ angles of 22.5° (100), 45.6° (200), and 71.4° (300). After annealing, the BFO films showed clear crystal formation at the same 2θ positions, with higher intensity and sharper peaks compared to the unannealed samples. This indicates that the BFO thin films formed crystalline structures on NSTO (100) single crystals and FTO substrates when processed by RF magnetron sputtering and heated at 600°C for 30 minutes. However, impurity phases from the NSTO and FTO substrates, caused by diffraction of Cu-Kβ radiation, were observed and marked with a "*" symbol.

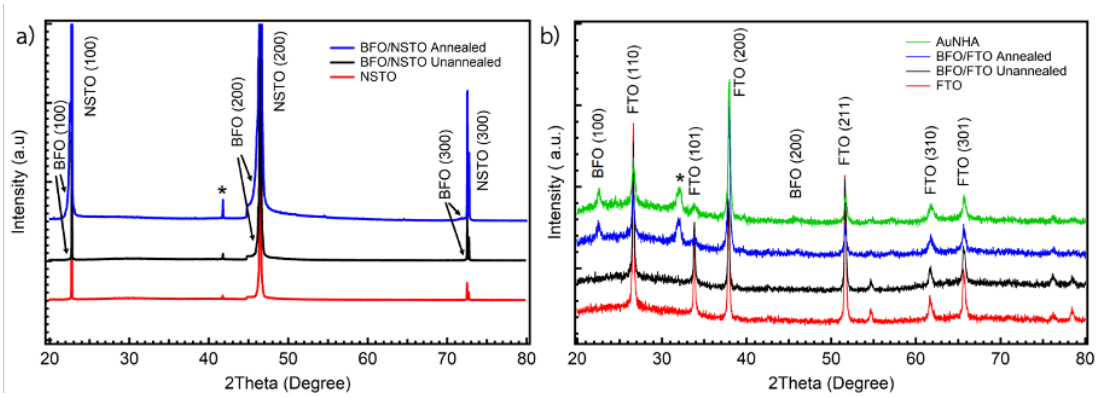

Figure 4.1 (a) shows the XRD patterns of NSTO, BFO/NSTO unannealed and annealed samples. (b) shows the XRD patterns of FTO, BFO/FTO unannealed and annealed samples, and AuNHA. The figure displays the (100), (200), and (300) diffraction peaks of BFO films on both substrates.

4.1.2 Scanning electron microscope (SEM)

SEM was used to observe the surface morphology of six sample conditions. The SEM high voltage was set at 20.0 kV for all images to ensure comparability. The images were taken with a magnification of 50 kx. For the NSTO substrate before adding any BFO, the surface appeared very smooth with no visible structures. This indicates that the NSTO was clean without crystal formations. Similarly, for the unannealed BFO/NSTO sample, the surface remained smooth, as illustrated in Figure 4.2(a) and Figure 4.2(b). This suggests that the BFO layer was thin and did not develop a crystalline structure. In contrast, the BFO/NSTO sample after annealing at 600°C for 30 minutes exhibited the crystallization on BFO thin film, suggesting that the heating process improves the formation of crystals as demonstrated in Figure 4.2(c).

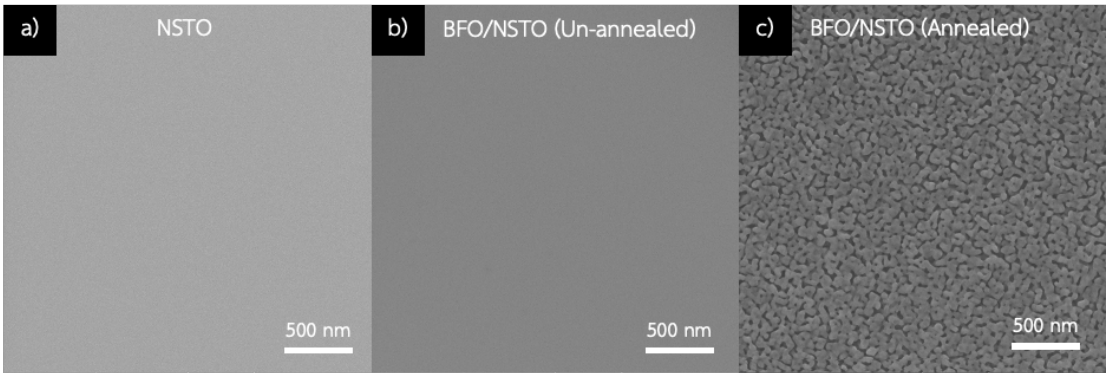

Figure 4.2 SEM images of (a) NSTO substrate, (b) BFO/NSTO sample in the RT condition with 3 minutes deposition time, (c) BFO/NSTO after annealing. The scale bar represents the length of 500 nanometers.

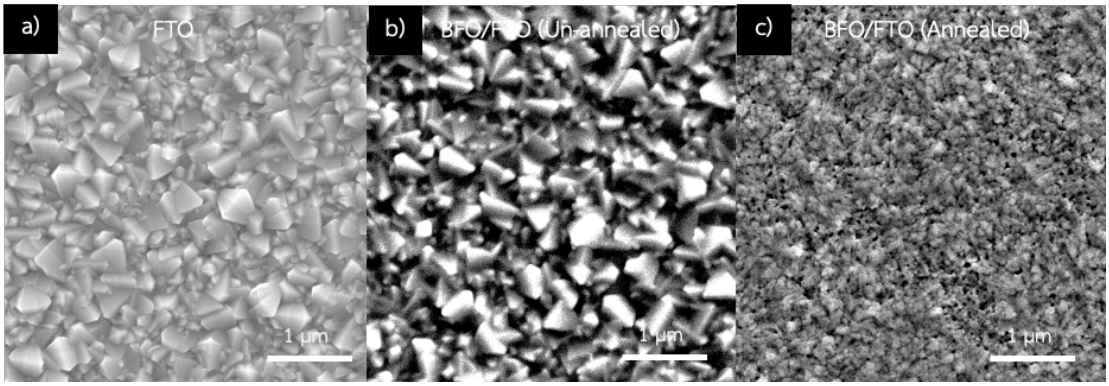

Figure 4.3 SEM images of (a) FTO substrate, (b) BFO/FTO sample in the RT condition at a deposition time of 3 minutes, (c) BFO/FTO after annealing. The scale bar represents the length of 1 micrometer.

For the FTO substrate samples, SEM images were taken at a magnification of 20 kx, and the high voltage was set to 10.0 kV. The surface morphology of the FTO substrate showed a grainy structure with well-defined grains (Figure 4.3(a)). This is typical for FTO glass, where the grains are relatively uniform in size and shape. The surface morphology of BFO deposited on FTO glass without annealing was more irregular and rougher compared to that of the FTO glass (Figure 4.3(b)). The grains appeared larger and less uniform, suggesting that the BFO layer was not well-

crystallized. In contrast, the surface morphology of BFO on FTO glass after annealing was smoother and more uniform compared to the unannealed sample. The grains were smaller and more evenly distributed, suggesting that the annealing process improved the crystallinity of the BFO layer (Figure 4.3(c)).

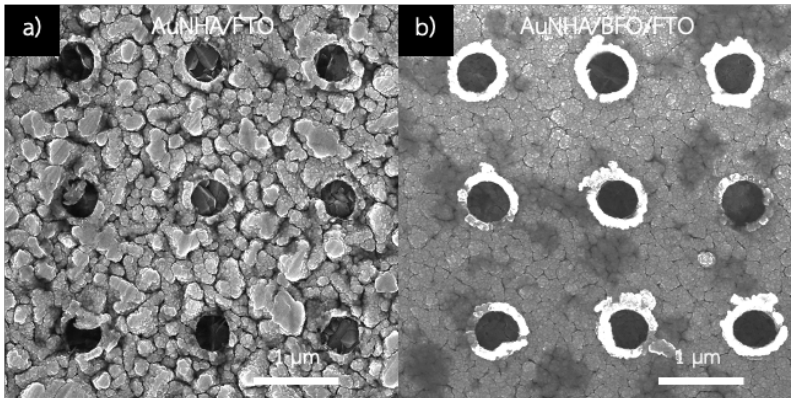

Figure 4.4 SEM images of AuNHA on (a) FTO substrate, (b) BFO/FTO sample in the RT condition at a deposition time of 3 minutes. The scale bar represents the length of 1 micrometer.

The surface morphology of AuNHA/FTO and AuNHA/BFO/FTO samples was observed using SEM images with a high voltage setting of 30.0 kV and a magnification of 30 kx. The nanoholes were arranged in a regular pattern, consistent in size and shape, indicating a precise and controlled fabrication process. The average size of the holes on FTO was 446 nm (Figure 4.4(a)). While the nanoholes of the AuNHA/BFO/FTO sample had an average hole size of 493 nm, as illustrated in Figure 4.4(b).

4.1.3 Field emission scanning electron microscope (FESEM)

After the sample preparation process, we used FIB to create grid patterns with size 200-2000 nm. For the PFM study, a dimension of 300x400 nm^2 was used because this size closely matches the AuNHA sample. The polarization on the surface is most clearly observed at this size. The acceleration voltage, ion current, and

depth were set at 30 kV, 200 pA, and 0.4 micrometers, respectively. The spot size of the probe was 30 nm. The ion beam was positioned at a 90 degrees angle to the surface being etched by rotating the sample stage by 54 degrees. FESEM was used to observe the surface morphology of the sample with SEM high voltage settings at 5.0 kV.

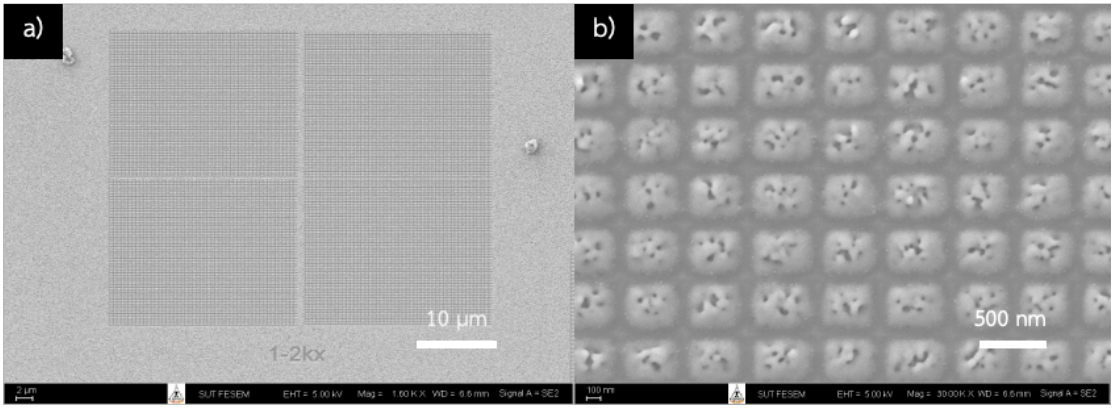

Figure 4.5 FESEM images after patterned nanostructures of unannealed BFO/NSTO. The magnified images of square-shaped nanostructures are shown at (a) 1.6 kx and (b) 30 kx. The patterning field size is 40 x 50 μm^2 and grids size is 300 x 400 nm^2. The scale bars represent 10 μm and 500 nm, respectively.

In figure 4.5(a), a nano grid pattern was created using FIB. The grid size is 300 x 400 nm², and the total patterned area is 40 x 50 µm². The grid was made with high precision and uniformity, demonstrating the capability of FIB to create small, accurate patterns. The overall area exhibits a well-ordered and consistent structure. A zoomed-in view of the same nano grid at a magnification of 30 kx as demonstrated in Figure 4.5(b). This close-up shows more details of the individual grid cells. Each cell appears uniform, although some imperfections are visible on the surface. These imperfections might be due to the deposition and annealing process. Despite these minor issues, the grid shows high precision and consistency, proving that FIB is effective for creating nanoscale patterns.

4.1.4 Energy dispersive X-ray spectroscope (EDS)

EDS was used to determine the weight and atomic percentages of elements in NSTO, BFO/NSTO, FTO, and BFO/FTO samples. The peaks in the graphs indicate the presence of elements in each sample. For the NSTO substrate, elements detected included Strontium (Sr), Titanium (Ti), Niobium (Nb), and Oxygen (O). Additionally, Bismuth (Bi) and Iron (Fe) were found in the BFO thin film on the NSTO substrate, both unannealed and annealed, with the weight and atomic percentages shown in Figures 4.6(a) to 4.6(c). For the FTO substrate, only Tin (Sn) and Oxygen (O) were found. Similar to the NSTO substrate, Bismuth and Iron were detected when the BFO layer was deposited on the FTO substrate, as illustrated in Figures 4.6(d) to 4.6(f). This confirms that the BFO layer was successfully deposited on both the NSTO and FTO substrates. Comparing the unannealed and annealed BFO/NSTO and BFO/FTO samples, there are slight differences in the weight and atomic percentages of the elements. The annealing process alters the material structure, affecting the distribution and percentage of elements.

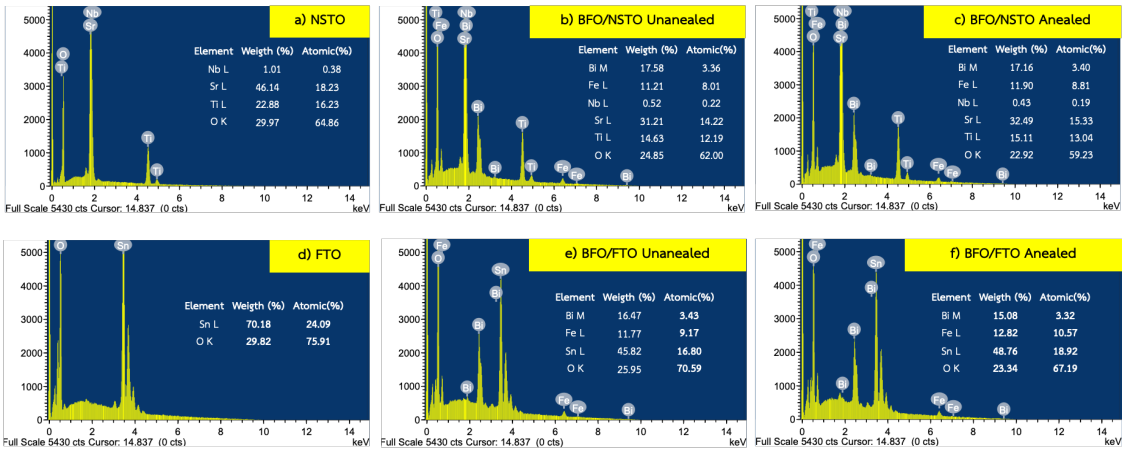

Figure 4.6 EDS elemental analysis of (a) NSTO substrate, (b) BFO/NSTO unannealed, (c) BFO/NSTO annealed, (d) FTO substrate, (e) BFO/FTO unannealed and, (f) BFO/FTO annealed.

4.2 Ferroelectric properties

To confirm the ferroelectric property, there are two effects that need to be checked. First, the domains should have different orientations of polarization. Second, there should be hysteretic switching between opposite domain states caused by electric fields. Hence, Piezo-respond Force Microscopy (PFM) was used in this experiment to study the ferroelectric properties of the BFO/NSTO and BFO/FTO samples and both un-patterned and patterned areas were studied. The tip applied voltage in the poling process was set to be +10V and -10V for all the PFM measurements. Additionally, we also studied the effect of UV irradiation on the ferroelectric properties.

4.2.1 Controlling the nano-scale ferroelectricity in unpatented area

To test the limitations of ferroelectricity control, we utilized PFM to create small-sized letters on a BFO/NSTO sample. In this experiment, we created the letters by applying a +10 V DC voltage over a 4 x 4 micrometer area and then applying -10 V to write the letters. After poling, the PFM amplitude and phase were investigated,

as shown in Figure 4.7. The PFM amplitude images show the letters "SUT" clearly visible, standing out from the background. The bright areas represent a strong response to the applied voltage, while the dark areas show a weaker response. The brightness ranges from 0 to 1.4 V, indicating the magnitude of polarization on the sample. The phase images display distinctly visible letters, representing changes in polarization direction, with phase values ranging from -80 to 80 degrees.

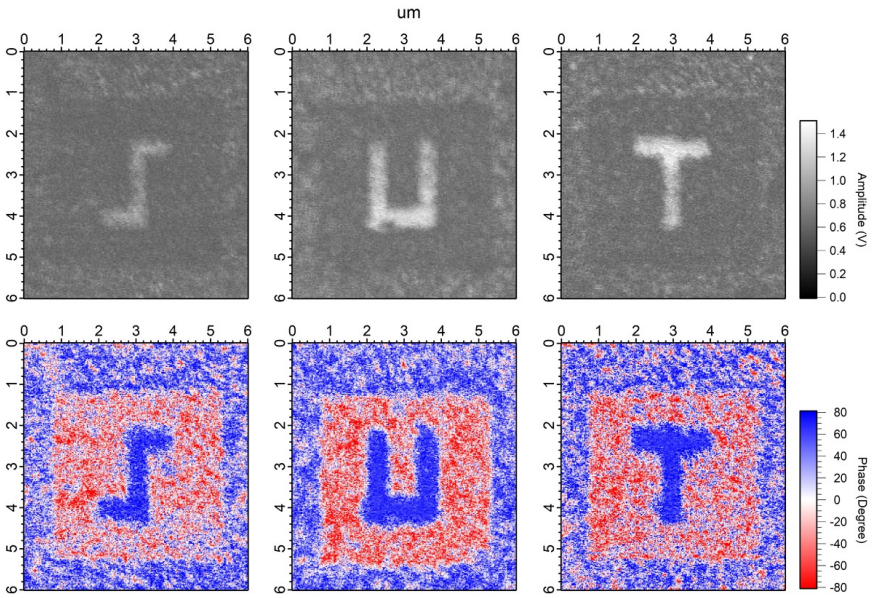

Figure 4.7 PFM images showing the nano-letter patterns on the BFO/NSTO annealed surface. The top row displays PFM amplitude images, and the bottom row shows PFM phase images. The letters S,U, and T were created by applying +10 V over a 4 x 4 micrometer area (red color) and then -10 V to form the letters, each approximately 500 nm wide (blue color). The scan size for each image is 6 micrometers.

From these experimental results, we conclude that we successfully used PFM to investigate these nano patterns and create tiny, polarized letters on the BFO/NSTO surface by applying different DC voltages. The letters are approximately 500 nm in size. The clear contrasts in the amplitude and phase images show that the electric fields effectively changed the local polarization states. The ability to create

and detect such small patterns can be useful for data storage and nano-electronic devices. It also aids in studying small-scale domain changes.

4.2.2 Effect of nanopatterning on ferroelectricity

For the un-patterned BFO/NSTO annealed sample, the hysteresis loop results and PFM images, including topography, amplitude, and phase, are shown in Figure 4.9. The topography image clearly shows the surface of the BFO film, identifying surface features of the sample (Figure 4.8(a)). The amplitude image distinctly shows different contrasts when an electric field is applied; higher amplitude indicates a stronger piezoelectric response. After poling, areas with different polarization states display varying amplitude levels, with magnitude ranging from 0 to 2.1 V (Figure 4.8(b)). The phase image effectively represents the direction of polarization. The contrast in phase helps identify areas with different polarization directions. After poling with +10V and -10V, distinct phase regions indicate domain switching (Figure 4.8(c)). The hysteresis loops for amplitude, phase, and piezo response over applied voltage are shown in Figures 4.8(d), 4.8(e), and 4.8(f), respectively. The amplitude loop shows the change in piezoelectric amplitude as the voltage is applied. The "butterfly" shape, typical of ferroelectric materials, demonstrates how the piezoelectric response changes with voltage, confirming the magnitude of polarization switching under an electric field. The phase loop shows the change in polarization direction as the voltage is applied. A typical ferroelectric phase hysteresis loop displays sharp phase changes, indicating the switch between polarization states. For the un-patterned area, the phase switched in the range from -80 to +80 degrees. The piezoresponse vs. applied voltage plot combines the amplitude and phase data to show the overall piezoelectric response of the sample. The results of this experiment reveal that BFO/NSTO annealed exhibits strong ferroelectric and piezoelectric properties in the un-patterned area, with clear domain switching and significant piezoelectric response under applied electric fields.

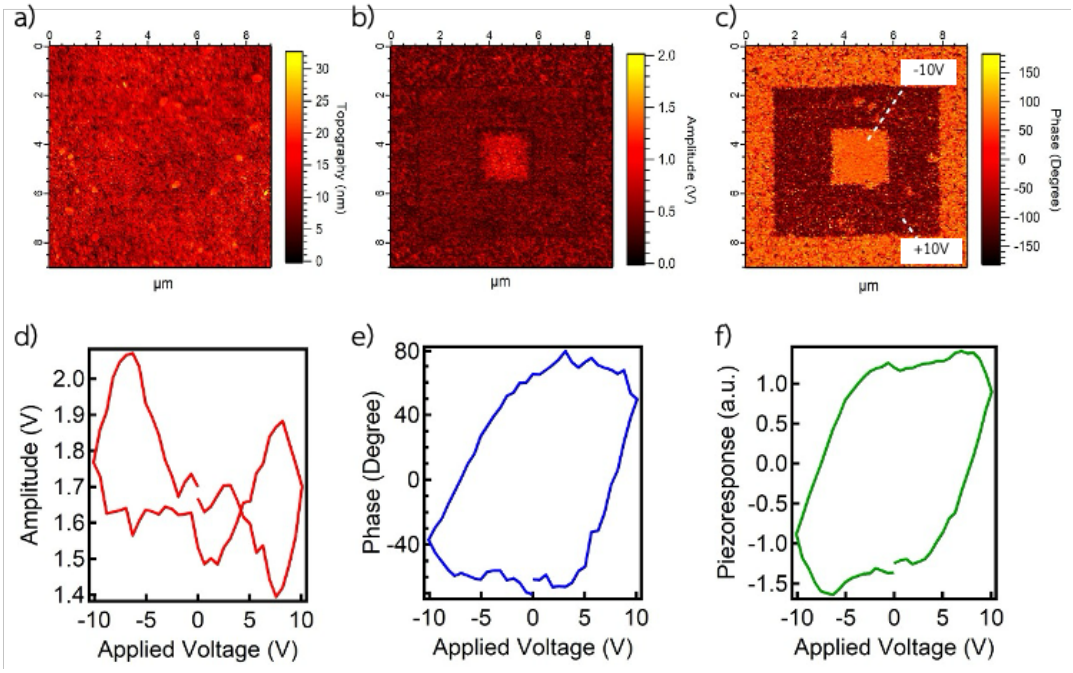

Figure 4.8 PFM Images for un-patterned area (a) the topography, (b) PFM amplitude, and (c) PFM phase images after poling with +10V and -10V DC voltages. The hysteresis loops of BFO/NSTO annealed in the un-patterned area (d) amplitude, (e) phase, and (f) piezoresponse as functions of applied voltage.

For the nano-scale grid patterned by FIB, Figure 4.9 presents the results of a PFM and hysteresis loop study on an BFO/NSTO annealed sample with a nano grid size of 400-500 nm. The topography image (Figure 4.10(a)) shows the surface features of the BFO film in a nano grid pattern, clearly indicating a well-defined structure created by the FIB technique. The grid features are approximately 300x400 nm^2 in size, with a height of around 80-100 nm. The amplitude image (Figure 4.9(b)) did not reveal clear contrast after poling, with the polarization magnitude measurable only in the range of 0-1.2 V. However, the phase image (Figure 4.9(c)), after applying +10V and -10V, displayed distinct phase regions, indicating successful domain switching within the grid pattern. The contrast in these phase regions confirms the presence of polarization domains. The hysteresis results, shown in Figures 4.9(d) to 4.9(f), confirm the ferroelectric properties of the nano grid pattern through the characteristic butterfly

shape in the amplitude and phase switching. The phase hysteresis loop shows a switch between positive and negative at around 60 degrees, which is less than the un-patterned area. Additionally, the clockwise rotation of this phase result compared to the unpatterned area indicates the involvement of an electrostatic field. The piezoresponse plot with the applied electric field further indicates ferroelectric properties in the nano grid pattern.

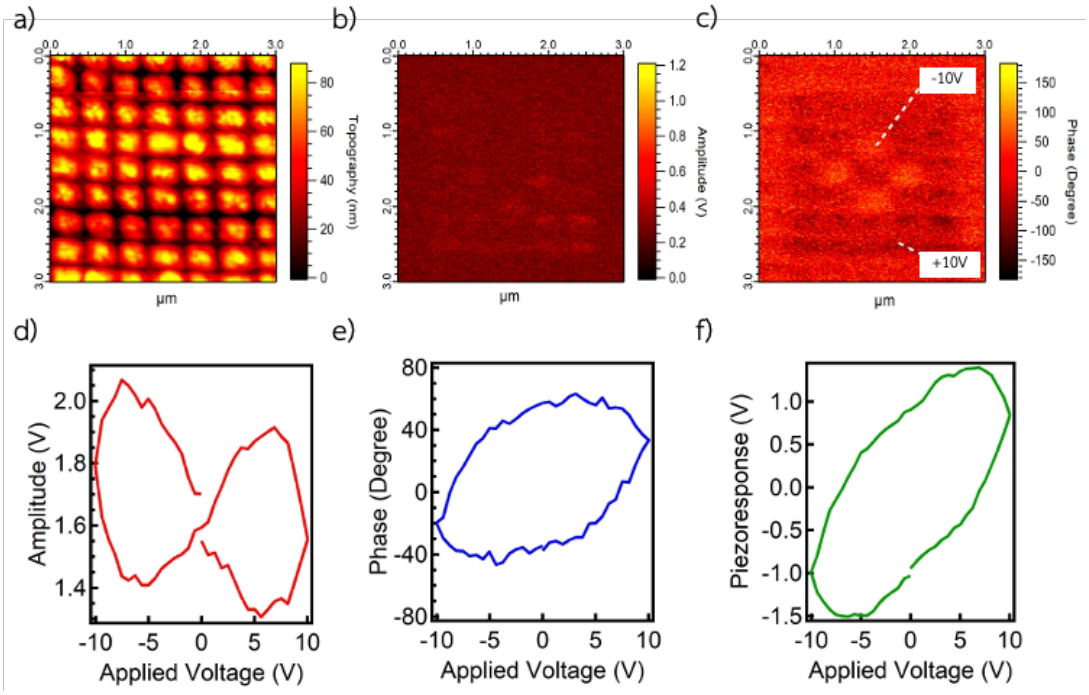

Figure 4.9 PFM and hysteresis loops of nano-grid BFO/NSTO. The top row displays (a) topography, (b) PFM amplitude, and (c) phase images after poling with +10V and -10V DC voltages on a grid. The hysteresis loops for (d) amplitude, (e) phase, and (f) piezoresponse over applied voltage.

For BFO/FTO annealed sample, topography Image (Figure 4.10(a)) reveals the surface features of AuNHA on BFO/FTO. The nanohole pattern is clearly visible, indicating successful fabrication of the nano-array with the average hole size of 493 nm. The amplitude (Figure 4.10(b)) and phase image (Figure 4.10(c)) represent the piezoelectric response of the sample only around the hole region. The contrast of

amplitude and the phase switching are not clear, suggesting low piezoelectric response across the nanohole array region. The PR curve combines amplitude and phase data to present the overall piezoelectric response of the sample. The piezoelectric responses of the material show smaller than 2 previous samples, demonstrating non-effective polarization switching within the nanohole array as illustrated in Figure 4.10 (e-f).

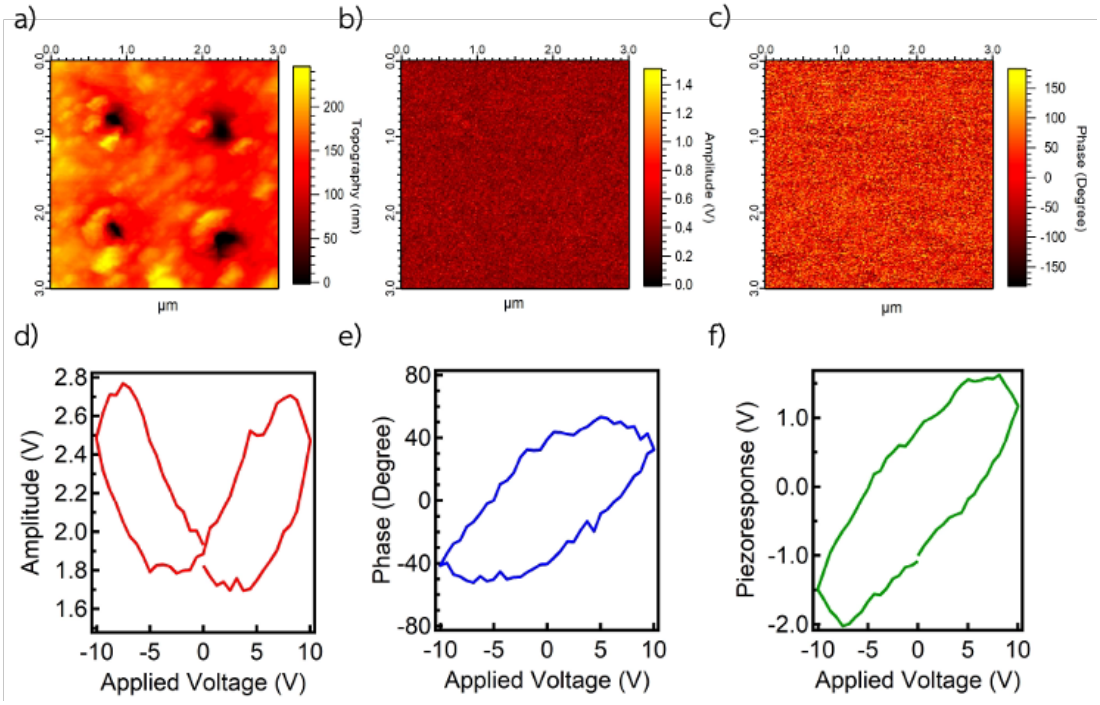

Figure 4.10 PFM and hysteresis loop AuNHA/BFO/FTO (hole size 493 nm). The top row displays (a) topography, (b) amplitude, and (c) phase images, revealing the surface features and polarization states after poling with +10V and -10V DC voltages. The hysteresis loops for (d) amplitude, (e) phase, and (f) piezoresponse vs. applied voltage.

Table 4.1 Ferroelectric coefficient.

Sample	Maximum Amplitude	Remnant Polarization (P_r)	Coercive Field (E_c)
Unpatterned Area	2.07 V	±1.2 V	±8.2 V
FIB Patterned Area	2.07 V	±0.9 V	±6.9 V
Nanohole Array Patterned Area	2.77 V	±0.83 V	± 6.3 V

The piezoelectric response and domain switching were observed in both the nanohole array and the FIB-patterned area. However, the unpatterned area exhibited a higher overall piezoresponse. From the piezoresponse hysteresis loops plot, we determined the remnant polarization and coercive field for these three areas, as shown in Table 4.1. The unpatterned area had larger piezoresponse values, but the patterned areas (both FIB and nanohole array) exhibited more consistent switching behavior.

4.2.3 Effect of UV irradiation on ferroelectricity

For this section, we will investigate the ferroelectric properties of an annealed BFO film on an NSTO substrate by measuring the PFM amplitude under three different UV irradiation states: state1 (No UV), state 2 (Under UV), and state 3 (After UV). Additionally, there are also three distinct areas (A1, A2 and A3) which extend it into nine conditions: ($A_{1,1}$) to ($A_{3,3}$) as illustrated in Table 4.2. The poling process was set to applied voltage -10 V and +10V into the sample. The average amplitude (mean) and standard deviation (SD) for each area were calculated and plotted against the UV states. All the results were shown in Figure 4.11 and Figure 4.12.

Table 4.2 UV irradiation conditions for -10V applied voltage.

State/Area	A1	A2	A3
1	Poling before UV ($A_{1,1}$)	-	-
2	Amplitude decay ($A_{1,2}$)	Poling with UV ($A_{2,2}$)	-
3	Amplitude decay ($A_{1,3}$)	Amplitude decay ($A_{2,3}$)	Poling after UV ($A_{3,3}$)

There are two sets of experiments: one with an applied voltage of -10V and the other with +10V. Firstly, the results in area A1 showed a significant drop in amplitude from 2.3V to 0.43V between conditions ($A_{1,1}$) and ($A_{1,2}$), indicating that UV exposure reduces the ferroelectric response. The amplitude then remains unchanged from condition ($A_{1,2}$) to ($A_{1,3}$). Notably, the amplitude of 0.63V in the ($A_{2,2}$) state suggests that the poling process under UV irradiation ($A_{2,2}$) is less effective compared to the poling without UV in the (A1,1) and ($A_{3,3}$) states. The amplitude slightly decreases from the ($A_{2,2}$) state to the ($A_{2,3}$) state, suggesting normal decay over time. Interestingly, the poling process after UV irradiation results in an amplitude increase similar to the ($A_{1,1}$) state, although the magnitude is slightly lower. This indicates that the ferroelectric properties do not fully recover to the initial state after UV exposure.

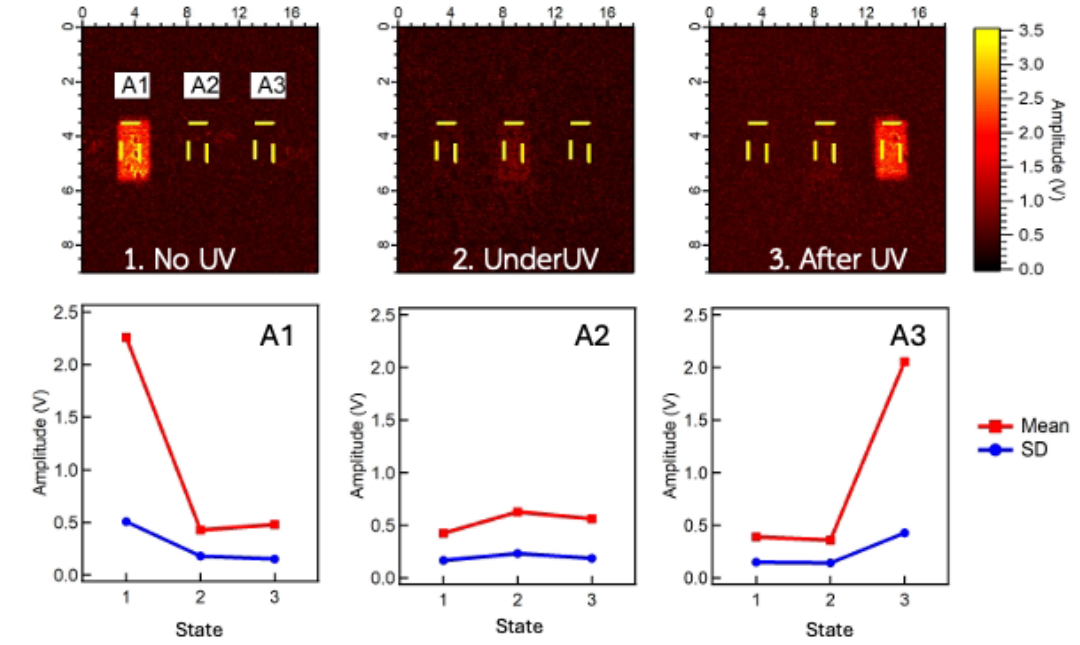

Figure 4.11 PFM amplitude measurements of BFO film on NSTO under different UV states (poling -10V) : No UV (State 1), Under UV (State 2), and After UV (State 3). The top row displays the PFM amplitude images for each state, while the bottom row shows the mean and standard deviation (SD) of the amplitude for three areas (A1, A2, and A3) across the different states.

In contrast, the effect of UV irradiation on the sample with -10V applied voltage is drastically different from the -10V condition discussed earlier. The amplitude between states ($A_{1,1}$) and ($A_{1,2}$) remains mostly the same, indicating that UV exposure no longer reduces the ferroelectric response. However, there is a significant decrease over time from state ($A_{1,2}$) to ($A_{1,3}$). Additionally, there is a notable difference between ($A_{2,2}$) for both -10V and +10V applied voltage states. For the +10V condition, a significant increase in amplitude is observed, whereas only a slight increase is found for the -10V condition. Similar to the trend observed between states ($A_{1,2}$) and ($A_{1,3}$), the decay over time from state ($A_{2,2}$) to ($A_{2,3}$) is also pronounced. Interestingly, in area A3, we found that the amplitude increases under UV irradiation even without applied voltage, from state ($A_{3,1}$) to ($A_{3,2}$). However, the poling process after UV irradiation

seems to be ineffective, as the amplitude remains mostly the same from state ($A_{3,2}$) to state ($A_{3,3}$).

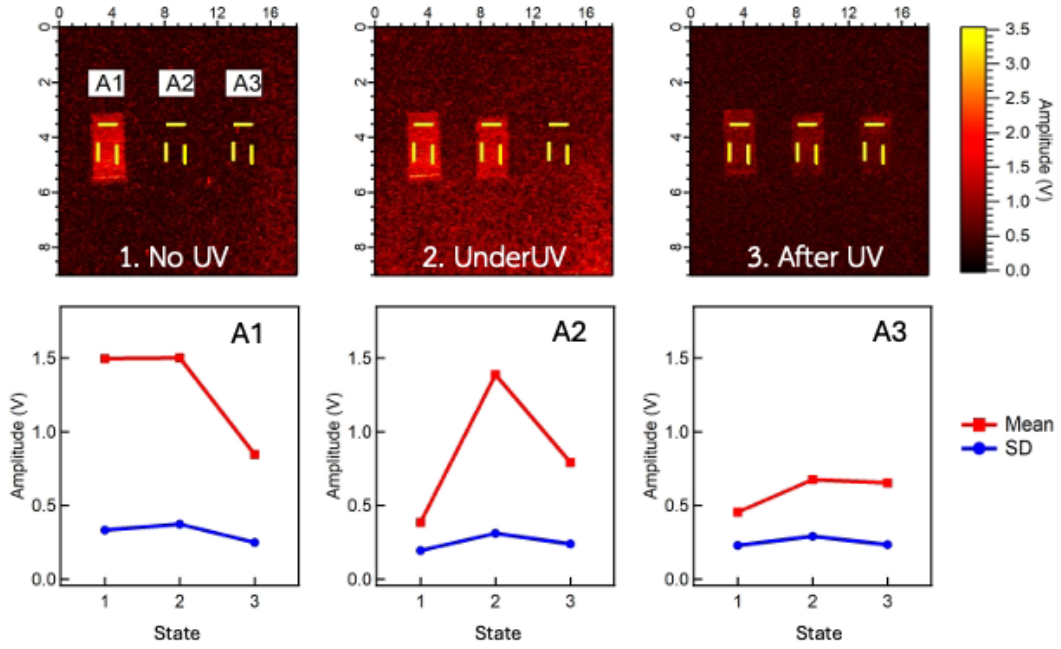

Figure 4.12 PFM amplitude measurements after +10V poling of BFO film on NSTO under different UV states: No UV (State 1), Under UV (State 2), and After UV (State 3). The top row displays the PFM amplitude images for each state, while the bottom row shows the mean and standard deviation (SD) of the amplitude for three areas (A1, A2, and A3) across the different states.

From earlier, we showed that UV exposure significantly reduces ferroelectric response due to photo-induced charge carriers, with partial recovery after UV removal. Differences in -10V and +10V poling conditions highlighted the role of the electric field in these changes. To deepen our understanding, we aim to investigate how varying UV exposure times affect the ferroelectric properties. The BFO/NSTO sample was also investigated using the PFM amplitude and phase over time under two conditions: No UV and Under UV. The poling voltage applied is -10V and +10V. The measurements were taken at intervals of 1, 2, 4, 6, 8, and 10 minutes under no UV

and UV on. The graphs display the mean (red line) and standard deviation (SD) in blue line of the amplitude and phase over time as illustrated in Figure 4.13.

For the -10V poling with No UV condition in the Figure 4.13(a) and Figure 4.14(c), the amplitude decreases steadily over time and shows a clear decline from the initial measurement, indicating a fading ferroelectric response. While the SD remains relatively low and stable. The phase remains stable over time, with minimal changes in both mean and SD values. This indicates that the polarization direction is maintained, despite the reduction in amplitude. However, the amplitude under UV condition in Figure 4.13(b) decreases rapidly within the first minute of UV exposure and continues to decline over time, but at a slower rate than the initial drop. This indicates that UV exposure accelerates the reduction in ferroelectric response. The SD remains low, like the No UV condition. In addition, the phase in Figure 4.13(d) shows slight changes and is less stable compared to the No UV condition, remaining relatively stable over time. The SD increases somewhat, indicating more variability in the phase under UV exposure.

For the +10V poling with No UV condition in the Figure 4.13(e) and 4.13(g), the amplitude drops significantly after the first minute and then it slightly increases from 2 minutes to 6 minutes. Additionally, it starts reducing again for the last 4 minutes with a small magnitude. The phase significantly increases in the first minute, then gradually reduces from 2 minutes to 8 minutes. The increasing of phase shows again at 10 minutes. In the case of UV exposure, the amplitude drops at the 1-minute mark of UV exposure, then increases at 2, 4, and 6 minutes, and drops again after 8 and 10 minutes as demonstrated in Figure 4.13(f) and 4.13(h). This pattern is very similar to the without UV exposure case; however, the magnitude is much stronger. This fluctuation indicates that UV exposure induces more dynamic changes in the amplitude compared to the No UV condition. The SD remains low, like the No UV condition. The phase trend is also like the without UV condition, showing initial

instability. Then, it positively changes after 8 minutes of UV exposure. The SD increases somewhat, indicating more variability in the phase under UV exposure.

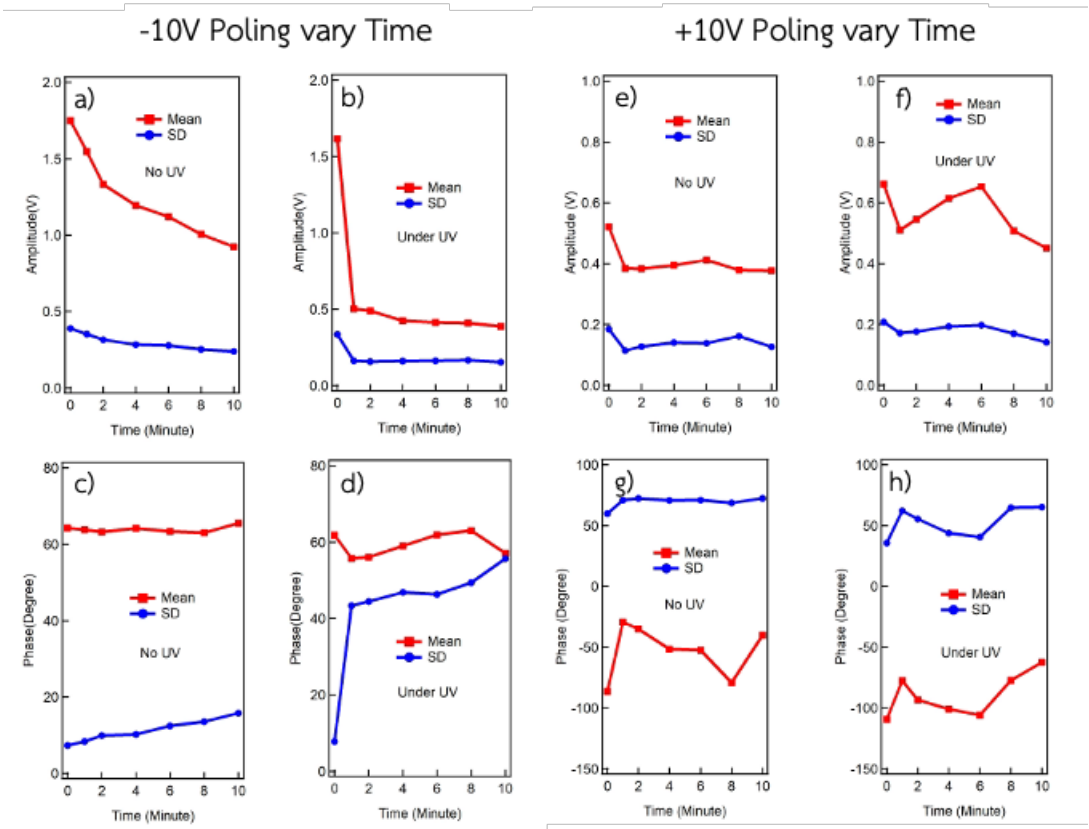

Figure 4.13 PFM amplitude and phase measurements of BFO/NSTO annealed over time with +10V and -10V poling under No UV and Under UV conditions.

From our result, we can suggest that both -10V and +10V poling conditions show a reduction in amplitude over time, especially under UV exposure. Notably, the reducing fashion of amplitude is similar between without UV and under UV irradiation with weak and strong magnitude, respectively. For -10V poling, the amplitude decreases steadily under No UV (decrease to 47%) and rapidly under UV (decrease to 76%). Moreover, the amplitude shows a significant decline under UV within the first minute and then stabilizes, indicating a fast initial response to UV exposure. For -10V poling, the amplitude drops significantly after the first minute under

No UV (down to 27.6 %) and then fluctuates with small margin. Under UV, the amplitude shows more dynamic changes (down to 31.7%), with strong fluctuations at different time points. The phase remains relatively stable in both conditions, with some fluctuations under UV exposure. For -10 V poling condition, the phase remains stable under No UV but shows slight variability under UV. While, for +10 V poling condition, the phase alternates between positive and negative values more prominently under No UV and stabilizes towards the end, while under UV, it shows greater variability and shifts to positive degrees at later times.

4.3 Polarization-Electric field Hysteresis Loop (P-E loop)

This study examines the ferroelectric properties of a BFO film (approximately 80 nm thick) on an NSTO substrate after annealing, using a P-E hysteresis loop to plot polarization (P) against the electric field (E). The graph presents three conditions: “No UV”, “Under UV”, and “After UV”. The gold top electrode size was 100 x 100 μm, and the bottom electrode was silver paste. The maximum voltage applied was ±1 V, corresponding to an electric field of ±200 kV/cm. The polarization of the samples was measured at 50 Hz, as shown in Figure 4.14. The P-E hysteresis loop under no UV exposure is oval-shaped, indicating both ferroelectric and resistive behavior. The remnant polarization (P_r), which is the polarization value at zero electric field, is 20.29 μC/cm² highest in this condition, showing strong ferroelectric properties. The coercive field (E_c), where the polarization switches direction, is 105.75 kV/cm, also highest in this condition. Under UV exposure, the P-E loop shows a shift from resistive to slightly ferroelectric behavior. Both the remnant polarization (4.81 μC/cm²) and coercive field (13.58 kV/cm) are reduced compared to the no UV condition. This reduction suggests that UV exposure introduces photo-induced charge carriers, affecting the material's ability to switch polarization and resulting in weaker ferroelectric properties. After UV exposure, the P-E loop shows partial recovery of the remnant polarization (17.45 μC/cm²) and coercive field values (79.35 kV/cm) compared to the Under UV

condition. This indicates that while some effects of UV exposure persist, the ferroelectric properties begin to revert to their original state once UV exposure stops. These findings highlight the influence of UV light on the ferroelectric behavior of BFO films and suggest potential for tunable ferroelectric properties through controlled UV exposure. This understanding is crucial for applications in optoelectronic devices and non-volatile memory where controlled switching of polarization states is required.

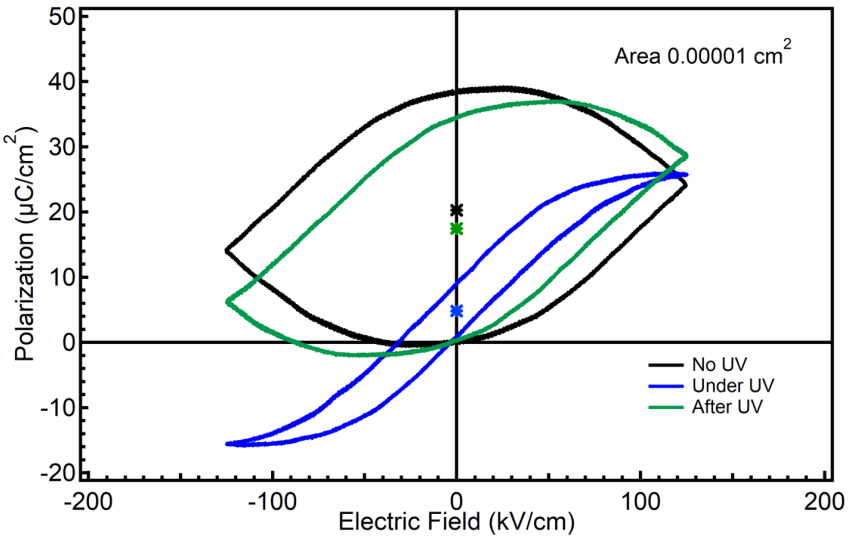

Figure 4.14 The P-E hysteresis loops of BFO/NSTO annealed under different conditions: No UV (black line), Under UV (blue line), and After UV (green line). The graph plots polarization (μC/cm²) versus electric field (kV/cm).

4.4 Voltage Response of Annealed BFO Film on NSTO Under Different UV Power Conditions

The voltage was measured between the top electrode and the bottom electrode with two conditions under UV exposure or without UV exposure. The results showed that the voltage remains relatively stable and close to 0 mV for all power levels when the UV is turned off. This indicates that without UV exposure, there is minimal photo-induced activity affecting the BFO film's voltage. On the other hand, the voltage rise is more significant at higher UV power levels, except for 0.3 mW which presents no response of the voltage. For the power of 14 mW (blue line), the voltage increases more noticeably, reaching approximately 0.7 mV. While the voltage can reach 2.4 mV when the power is 25 mW. This behavior indicates that higher UV power results in a greater photo-induced voltage response in the BFO film. When the UV is turned off again, the voltage decreases back to nearly 0 mV for all power levels. This decrease shows that the photo-induced effects are reversible and that the BFO film returns to its initial state when UV exposure is removed. The consistent increase in voltage when sample is under UV irradiation and the decrease without UV across all power levels confirm that UV exposure induces a reversible photo-voltaic effect in the BFO film. The effect is more pronounced with higher UV power.

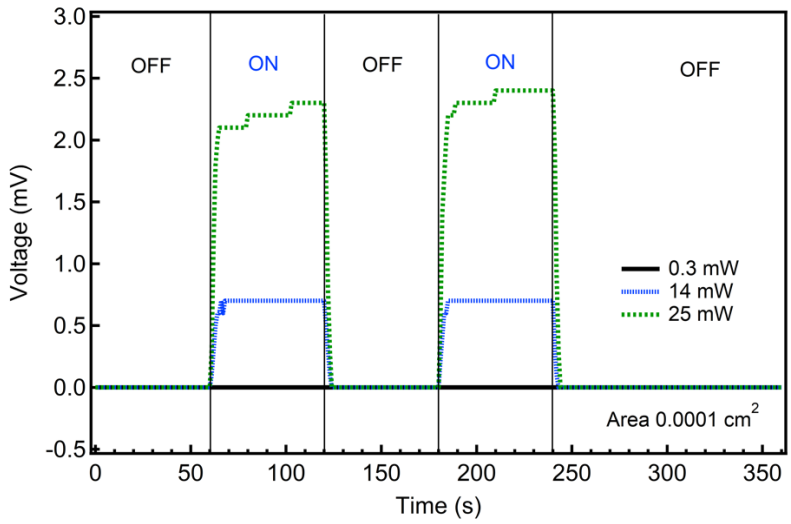

Figure 4.15 Voltage response over time for annealed BFO film on NSTO under different UV power conditions. The voltage was measured between the top and bottom electrodes. The graph shows the voltage response for UV power levels of 0.3 mW (black line), 14 mW (blue line), and 25 mW (green line). The voltage increases with UV ON and decreases with UV OFF, with higher UV power resulting in a greater photo-induced voltage response.